Dalton Transactions

ROYAL SOCIETY OF CHEMISTRY

PAPER

View Article Online
View Journal | View Issue

Cite this: *Dalton Trans.*, 2025, **54**, 15745

Bimetallic platinum(II) complexes with bridging di-NHC and N^C^C ligands: synthesis and photophysical properties

Mariano Paredes, Dionisio Poveda, Pablo González-Herrero and Ángela Vivancos *

Three new bimetallic Pt(II) compounds of the type [{Pt(dmtppy)}$_2${μ-(Im$_{Me}$)$_2$(CH$_2$)$_n$}] [n = 1 (**1**), 3 (**2**), 6 (**3**)], where dmtppy is the dimetalated tridentate N^C^C ligand 2-(4,4″-dimethyl-[1,1′:3′,1″-terphenyl]-5′-yl) pyridine and Im$_{Me}$ is *N*-methylimidazol-*N*-yl-2-ylidene, have been synthesized in order to explore their ability to form molecular assemblies that affect their luminescence. Restricted rotation around the Pt–carbene bond leads to mixtures of atropisomers, which hinder the growth of single crystals. The complexes show efficient emissions with high phosphorescence quantum yields in 2 wt% doped PMMA films at 298 K (PLQY: 73–77%). Significant modifications of their photophysical properties in fluid solution are observed upon variation of the solvent, with the highest efficiencies found in 2-methyltetrahydrofurane (up to 63% quantum yield for complex **3**). In the case of complex **1**, which contains the shortest linkage, the formation of excimers in MeCN and MeOH causes a significant quenching of the emission, with a substantial decrease in the quantum yield.

Received 25th July 2025,
Accepted 26th September 2025

DOI: 10.1039/d5dt01761k

rsc.li/dalton

Introduction

The luminescence of Pt(II) complexes bearing cyclometalated 2-arylpyridines and related heteroaromatic ligands has been widely explored, enabling their use in different applications such as chemosensors, biological probes for cell imaging, or phosphors for organic light-emitting devices.[1–3] Their photophysics are highly influenced by the chelating and ancillary ligands and can be also affected by the formation of molecular assemblies, that can be built through metallophilic Pt···Pt contacts, intra- or intermolecular π-stacking or other non-covalent interactions. These aggregation phenomena can have a beneficial effect on their luminescence, with an enhancement of their emissions (aggregation-induced phosphorescence emission)[4,5] or, on the contrary, can cause the quenching of the luminescence (aggregation-caused quenching).[6] If the formation of aggregates is influenced by the environment, the complexes can be potentially useful for the design of chemical sensors.[7–13]

In recent years, a large variety of multinuclear complexes, containing two or more Pt(II) centers or a combination of Pt(II) and other platinum-group metal ions, have been studied to understand how interactions between the different metals affect their photophysical properties.[14–17] Among them, a great number of bimetallic Pt(II) species have been reported, most of them containing bidentate cyclometalated 2-arylpyridine (C^N) or aryl-N-heterocyclic carbene (aryl-NHC) ligands, along with two bidentate ligands that bridge the two platinum subunits.[18–23]

The rigidity and planarity of tridentate ligands have been shown to confer exceptional stability and luminescence characteristics, often resulting in improved emission efficiency, tunability, and robustness of the resulting complexes. In addition, the fourth coordination position can be employed to control their electronic properties and to design multinuclear complexes by introducing bridging ligands, which can lead to intramolecular non-covalent interactions between the metal subunits, with valuable possibilities for luminescence modulation and applications. The high interest in such strategy is reflected in the considerable number of bimetallic Pt(II) complexes with tridentate ligands, including terpyridine-type ligands[24–26] and other tridentate N^N^N ligands,[26] monocyclometalated N^N^C ligands derived from 6-phenyl-2,2′-bipyridine[27–30] or N^C^N ligands derived from 1,3-di(2-pyridyl)benzene-type proligands.[31,32] Dimetalated C^N^C ligands have also been employed, which have allowed the design of multinuclear stacked systems based on extended metal–metal and π–π interactions and the development of molecular tweezers with alkynyl-bridging ligands.[33]

Platinum complexes with N-heterocyclic carbene ligands (NHCs) have been extensively studied for different therapeutic

Departamento de Química Inorgánica, Facultad de Química, Universidad de Murcia, Campus de Espinardo, 19, 30100 Murcia, Spain. E-mail: angela.vivancos@um.es

applications.[34,35] In this respect, a few examples of bimetallic platinum species bearing a di-NHC have been reported,[28,36,37] but only one phosphorescent bimetallic platinum complex with a di-NHC bridge, of the type [{(C^N^N)Pt}$_2$(μ-di-NHC)], has been reported to date.[28] Due to the strong σ-donor ability of NHCs, these ligands have been employed for the design of highly efficient luminescent transition-metal complexes. NHCs enhance the stability of the complexes by inducing large ligand-field splittings, thereby elevating the energies of dissociative, metal-centered (MC) excited states and diminishing the nonradiative deactivation that occurs due to the thermal population of such states.[38–40]

Usually, increasing the number of carbon-donor ligands bonded to the metal center leads to complexes with higher emission efficiencies, and in this regard dimetalated, tridentate N^C^C ligands derived from 2-(3,5-diarylphenyl)pyridines have emerged as excellent candidates for the design of luminescent species. They provide rigidity and a strong σ-donation from *cis*-arranged aryl groups, as well as planarity to allow aggregation phenomena. Although a few series of efficient Au(III)[41–43] and Pd(II)[44,45] emitters bearing tridentate heteroaromatic N^C^C ligands have been reported, only recently have luminescent Pt(II) complexes with ligands of this kind started to be developed. Thus, we have described a photochemical procedure for the synthesis of Pt(II) species with tridentate N^C^C ligands[46] and demonstrated that the introduction of different ancillary ligands at the fourth coordination position allows the modulation of their photophysical properties through the formation of molecular assemblies. This effect is particularly remarkable when the N^C^C ligand is a highly planar system, such as 2-(4,4″-dimethyl-[1,1′:3′,1″-terphenyl]-5′-yl)pyridine (dmtppy), and the ancillary ligands are isocyanides or CO, which lead to assemblies that present short Pt···Pt metallophilic contacts and produce red-shifted emissions from triplet metal–metal to ligand charge-transfer (^{3}MMLCT) excited states.[47] For the present work, we aimed to explore the platform {Pt(dmtppy)} for the development of dinuclear species with di-NHC bridging ligands. Structural characterization and photophysical properties are presented.

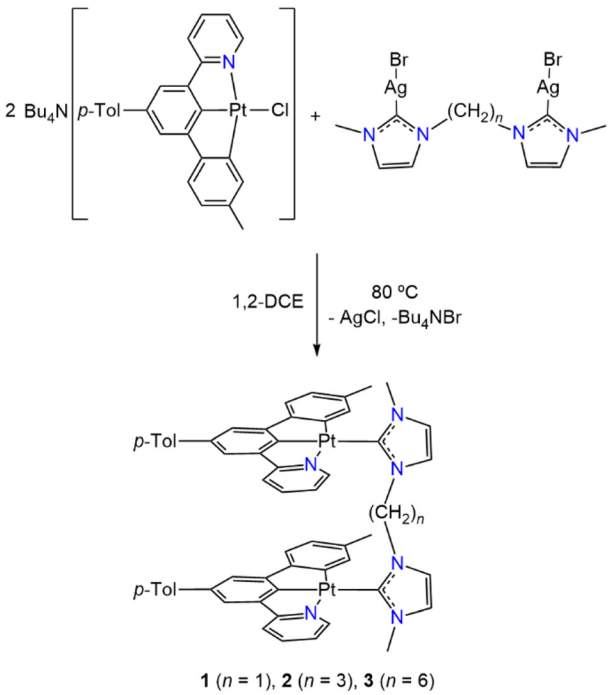

Scheme 1 Synthesis of complexes **1–3**.

Results and discussion

Synthesis and characterization

The synthesis of dinuclear complexes [{Pt(dmtppy)}$_2${μ-(Im$_{Me}$)$_2$(CH$_2$)$_n$}] [n = 1 (**1**), 3 (**2**), 6 (**3**)] was carried out by reacting the chloride precursor Bu$_4$N[Pt(dmtppy)Cl] with the silver carbene species [Ag$_2$Br$_2${μ-(Im$_{Me}$)$_2$(CH$_2$)$_n$}] (*N*-methylimidazol-*N*-yl-2-ylidene, n = 1, 3, 6) in 2 : 1 molar ratio (Scheme 1). When the transmetallation reaction was performed at room temperature, low yields were obtained, probably due to solubility problems. This was solved by heating the mixture at 80 °C in 1,2-dichloroethane for 2 h, which led to complexes **1–3** in good yields (55–63%) after filtration through silica gel.

The ^{1}H NMR spectra of the dinuclear species **1–3** show two sets of signals attributable to the presence of two different atropisomers in *ca.* 1 : 1 ratio, which arise due to restricted rotation around the Pt–carbene bond.[48–51] The presence of two stereoisomers is also revealed by the ^{13}C NMR spectra, where duplicated resonances are found for most of the signals, including those corresponding to the aliphatic linkers, *e.g.* 62.5 and 62.4 ppm for the methylene bridge in **1** and 32.0 and 31.9 ppm for the central methylene of the propylene linker in **2**. The ^{1}H NMR spectrum of complex **1**, with a methylene bridge between the imidazolylidene rings, exhibits broadened signals that we attribute to hindered rotation about the methylene linker, caused by steric interactions between the {Pt(dmtppy)} subunits that reduce its flexibility.

Variable temperature ^{1}H NMR measurements of complexes **1** and **2** in DMSO-d_6 solution (Fig. 1 and S8–S11) show that interconversion between isomers is not perceptible from 298 to 358 K. However, the spectra are temperature dependent, particularly in the case of **1** (Fig. 1), for which there are some resonances that are down- or upfield-shifted (*e.g.* from 7.76 ppm at 298 K to 7.68 ppm at 358 K) and the broad resonances observed at room temperature are resolved upon heating; *e.g.* from a broad signal at 7.18 ppm to doublet of doublets of doublets at 358 K that is slightly upfield shifted (7.15 ppm). These variations are likely due to faster rotations involving the aliphatic linker at higher temperatures, which lead to sharper resonances, as well as to subtle changes in the environment of the corresponding protons, whose proximity to aromatic rings in the complex may affect their shielding.

Enriched fractions in each of the atropisomers of **1** could be obtained through column chromatography in silica gel using a 9 : 1 mixture of diethyl ether and chloroform as eluent, which allowed us to obtain the ^{1}H and ^{13}C NMR data of the

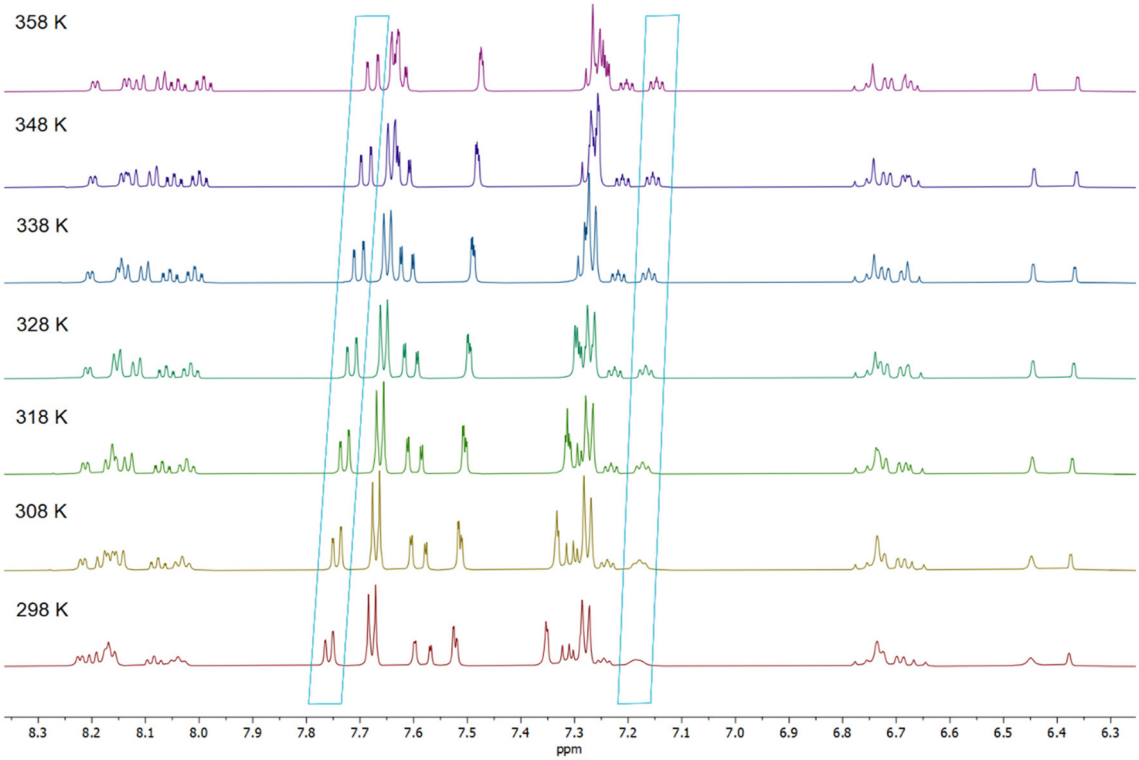

Fig. 1 Aromatic region of the ^{1}H NMR spectra of complex **1** (DMSO-d_6, 600 MHz, 298 to 358 K).

individual isomers, that we arbitrarily label as **1a** and **1b**. This separation was only possible using small amounts of the complex. Moreover, interconversion between them was observed to slowly take place in solution at room temperature. Thus, the first fraction eluted from the column was a mixture enriched in isomer **1a**, with a *ca.* 5 : 1 ratio between atropisomers (**1a** : **1b**; Fig. 2, top). Its ^{1}H NMR spectrum shows a characteristic broad doublet at 8.13 ppm and a singlet with platinum satellites at 6.49 ppm (J_{PtH} = 73 Hz), which are attributable to the CH *ortho* to the coordinated N atom and the metalated carbon of the *p*-tolyl ring, respectively (Fig. 2, top). After 72 h in CH_2Cl_2 solution, this mixture evolved to a 2.5 : 1 ratio (**1a** : **1b**) (Fig. S12). The ^{1}H NMR spectrum of the second eluted fraction showed a 1 : 9 ratio between **1a** and **1b** (Fig. 2, bottom) and after 24 h in solution it returned to 1 : 1.1 ratio (Fig. S13). For isomer **1b**, the CH *ortho* to the metalated carbon can be distinguished as a broad singlet at 6.62 ppm flanked by platinum satellites (J_{PtH} = 71 Hz).

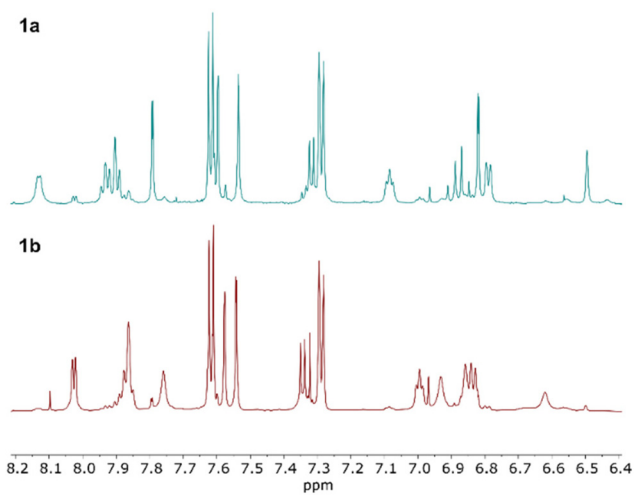

Fig. 2 ^{1}H NMR section (CD_2Cl_2, 600 MHz) of enriched fractions in atropisomers **1a** (top) and **1b** (bottom).

Attempts to separate the atropisomers of complexes **2** and **3** were unsuccessful. Therefore, their NMR data correspond to a 1 : 1 mixture of the two isomers in both cases (Fig. S4–S7). In contrast to the ^{1}H NMR spectra of **1**, no broad resonances are observed for complexes **2** and **3**. In the case of **2**, the presence of atropisomers is evidenced in its ^{1}H NMR spectrum by the appearance of several duplicated signals, *e.g.* the two singlets with satellites at 6.49 and 6.42 ppm (J_{PtH} = 73 Hz) that correspond to the CH *ortho* to the metalated carbon of the tolyl ring. Furthermore, two resonances at −3823 and −3825 ppm can be observed in the ^{195}Pt{^{1}H} NMR spectrum. Similarly, in the ^{1}H NMR spectrum of complex **3**, the isomers give rise to a singlet with platinum satellites at 6.48 and 6.46 ppm.

Attempts to obtain single crystals of **1–3** suitable for X-ray diffraction were unsuccessful, probably due to the presence of two atropisomers. To get a visualization of their possible molecular structure and the mutual arrangement of {Pt(dmtppy)} units, DFT optimizations were carried out for the two atropi-

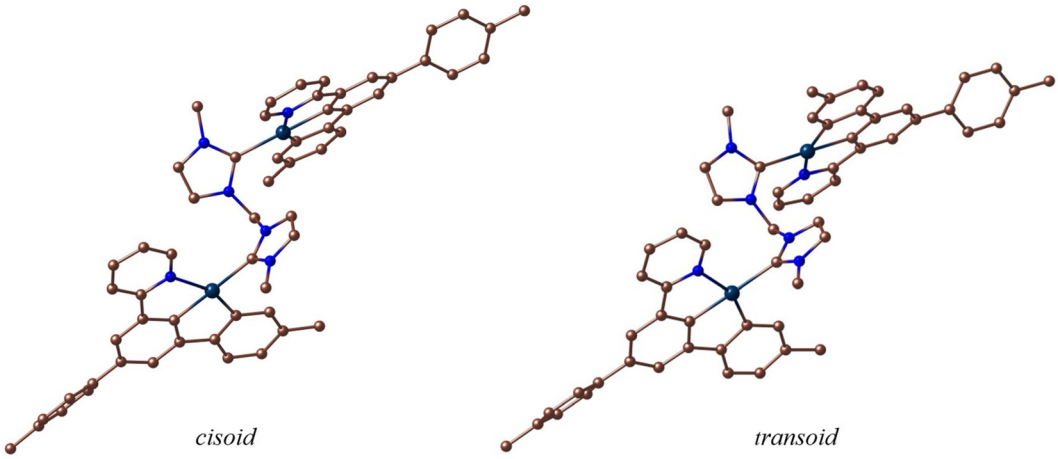

Fig. 3 Representations of the minimum energy geometries of the two possible atropisomers of complex **1** from DFT calculations.

somers of **1** that arise as a consequence of restricted rotation about the Pt–carbene bond. The representations of their optimized geometries are shown in Fig. 3, labeled as *cisoid* and *transoid* on the basis of the relative arrangement of the {Pt(dmtppy)} units. The imidazolylidene rings are rotated by 180° relative to each other, and the {Pt(dmtppy)} units are directed toward opposite directions, preventing the establishment of intramolecular interactions between them. The calculated free energies differ in only 0.6 kcal mol^{-1}, the *cisoid* isomer being thermodynamically more stable. This small energy difference explains why they are obtained as almost equimolar mixtures after the synthetic procedure.

Photophysical properties

The electronic absorption spectra of **1–3** were recorded in 2-methyl tetrahydrofuran (2-MeTHF) solutions at 298 K and

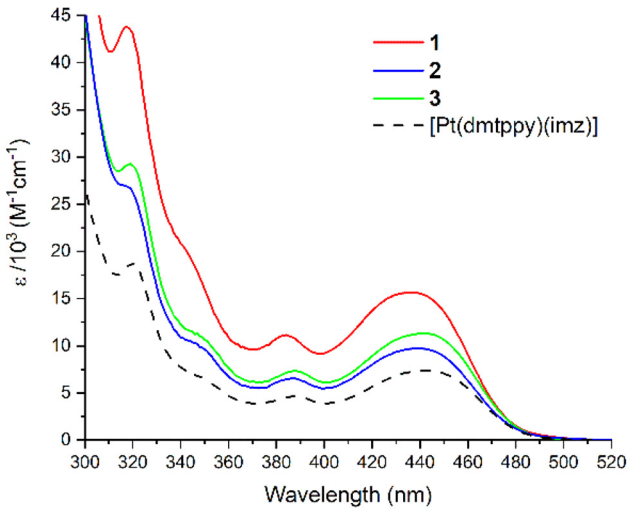

Fig. 4 Electronic absorption spectra of complexes **1–3** (*ca.* 2.5 × 10^{-5} M) and [Pt(dmtppy)(imz)] (*ca.* 5 × 10^{-5} M) in 2-MeTHF at 298 K.

Table 1 Electronic absorption data for complexes **1–3** (*ca.* 2.5 × 10^{-5} M) and [Pt(dmtppy)(imz)] (*ca.* 5 × 10^{-5} M) in 2-MeTHF solutions at 298 K

Complex	λ_{max}/nm ($\varepsilon \times 10^{-3}$ M^{-1} cm^{-1})
1	318 (44), 344 (20), 384 (11), 437 (16)
2	319 (27), 348 (10), 387 (6), 440 (10)
3	319 (29), 349 (11), 389 (7), 443 (11)
[Pt(dmtppy)(imz)]	319 (19), 349 (7), 387 (5), 443 (7)

are shown in Fig. 4 and the data are summarized in Table 1. The spectrum and data of the mononuclear derivative [Pt(dmtppy)(imz)][47] (imz = 1-butyl-3-methylimidazol-2-ylidene) are included to facilitate comparison. All complexes show nearly identical profiles, with four absorption bands around 319, 345, 385 and 440 nm, which are very similar to those found for the mononuclear complexes [Pt(dmtppy)(NHC)], with NHC = imz or 4-butyl-3-methyl-1-phenyl-1*H*-1,2,3-triazol-5-ylidene (trz).[47] According to our previous study, the two lowest-energy absorption bands arise from singlet intraligand charge-transfer (^{1}ILCT) transitions with metal-to-ligand charge-transfer character (^{1}MLCT).

To corroborate the charge-transfer character of the lowest-energy bands, additional absorption spectra of complex **3** were registered in solvents of different polarity, namely acetone, MeOH, MeCN and DMSO (Fig. 5 and Table 2). Significant shifts of the lowest band are observed, with λ_{max} values between 428 nm in MeOH and 442 nm in 2-MeTHF. Despite the fact that these variations are not well correlated with solvent polarity, they demonstrate that the stabilization of the excited and ground states is affected by solvation, which is typical of charge-transfer transitions involving a change in the polarity of the molecule. A similar behavior was observed for the mononuclear complex with the same N^C^C ligand and a NHC of the triazolylidene type.[47]

The photostability of complex **3**, as a representative of the series, was evaluated in MeCN, 2-MeTHF and MeOH by

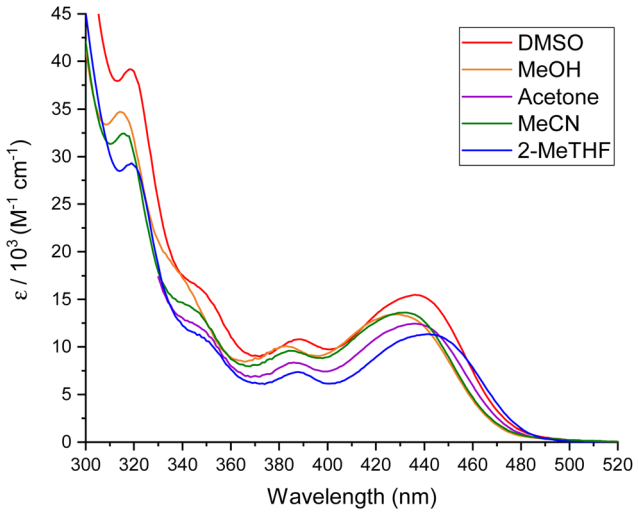

Fig. 5 Electronic absorption spectra of complex **3** in different solvents (*ca.* 2.5 × 10^{-5} M) at 298 K.

Table 2 UV-visible absorption data of complex **3** in solvents of different polarity (*ca.* 2.5 × 10^{-5} M) at 298 K

Solvent	λ_{max}/nm ($\varepsilon \times 10^{-3}$ M^{-1} cm^{-1})
2-MeTHF	319 (29), 349 (11), 389 (7), 443 (11)
Acetone	347 (12), 386 (8), 436 (12)
MeOH	315 (35), 339 (18), 382 (10), 428 (14)
MeCN	316 (32), 342 (14), 385 (10), 432 (14)
DMSO	319 (39), 348 (16), 389 (11), 437 (15)

measuring the absorption spectra of the corresponding deoxygenated solutions before and after irradiating them at 430 nm for 30 minutes. The absorbance profiles in MeCN and MeOH do not show any variation after irradiation (Fig. S14 and S15, respectively). However, in a 2-MeTHF solution, a slight decrease in the absorbance of the lower-energy band is observed after 30 minutes of irradiation, although no further changes occur if the solution is irradiated for 30 additional minutes (Fig. S16). Probably, traces of oxygen are the cause of this change. This is supported by the observation that aerated 2-MeTHF solutions of complexes **1–3** gradually lose their yellow color over time, possibly due to photooxidation.

The emission properties of complexes **1–3** were studied in MeCN, 2-MeTHF and MeOH solutions, as well as in PMMA matrices. All measurements were performed in the absence of oxygen at room temperature. The emission spectra in solution are shown in Fig. 6(a–c), and the data are summarized in Table 3. The emission data for the mononuclear complex [Pt(dmtppy)(imz)][47] have also been included for comparison. The complete set of excitation and emission spectra is included in the SI.

The emission of complex **1** in solution and PMMA shows some vibronic structure, with the highest-energy peak within the 524–529 nm range. In addition, a broad, red-shifted band is observed for **1** in MeCN (670 nm) and MeOH (678 nm) solution, being more intense in MeCN. The excitation spectrum monitored at this band matches the absorption spectrum, supporting its assignment to excimer formation. To further probe its origin, emission spectra of **1** were recorded in MeCN at concentrations ranging from 1.25 × 10^{-4} to 0.5 × 10^{-6} M (Fig. 6d). At the highest concentration, the relative intensity of the red-shifted band is pronounced, but it decreases upon dilution, consistent with intermolecular excimer formation. However, its persistence at low concentrations—with comparable relative intensity even after a fivefold dilution (from 2.5 to 0.5 × 10^{-6} M)—indicates the additional presence of intramolecular excimers involving {Pt(dmtppy)} subunits within the same molecule. Therefore, both intra- and intermolecular excimers contribute to the emission at 670 nm. In MeCN and MeOH solution, complexes **2** and **3** present similar emission profiles with a unique emission band at *ca.* 524 nm with some vibronic structure. However, in 2-MeTHF the emission is slightly red-shifted and is not vibronically structured. Lifetimes in the μs range demonstrate the triplet multiplicity of the emitting state, which can be described as mixed ^{3}ILCT/MLCT based on the previous assignment of the luminescence of Pt(II) complexes with N^C^C ligands.

Quantum yields in solution are strongly influenced by the solvent. Compound **1** shows markedly weaker emissions in MeCN and MeOH compared to 2-MeTHF, which can be attributed to efficient quenching through excimer formation. The highest quantum yields are obtained in 2-MeTHF, where none of the complexes display observable excimer formation. Within this medium, complex **3** exhibits the highest efficiency of the series (Φ = 0.63), a value slightly lower to that found for the mononuclear analogue [Pt(dmtppy)(imz)].

An analysis of the radiative and non-radiative rate constants (k_r and k_{nr}, respectively) in all solvents reveals a pronounced influence of linker length on k_{nr}, which decreases as the linker becomes longer. We attribute this trend to the ability of extended linkers to reduce non-radiative deactivation pathways arising from intramolecular collisions between {Pt(dmtppy)} subunits that do not generate emissive species. The effect on quantum yields is most clearly observed in 2-MeTHF, where the absence of detectable excimer formation isolates the linker-length contribution, resulting in a systematic increase across the series: **1** (0.39) < **2** (0.47) < **3** (0.63). The lower k_{nr} and higher quantum yield exhibited by the monomeric complex [Pt(dmtppy)(imz)] in this medium further corroborate the observed trend.

When the complexes are immobilized in PMMA, non-radiative decay due to intramolecular collisions between {Pt(dmtppy)} subunits is avoided and linker length does not have a perceptible influence. The three complexes exhibit high quantum yields in this medium (0.73–0.77), with similar emission profiles and lifetimes around 14 μs. These values are comparable to the data found for the monomeric complex [Pt(dmtppy)(imz)].

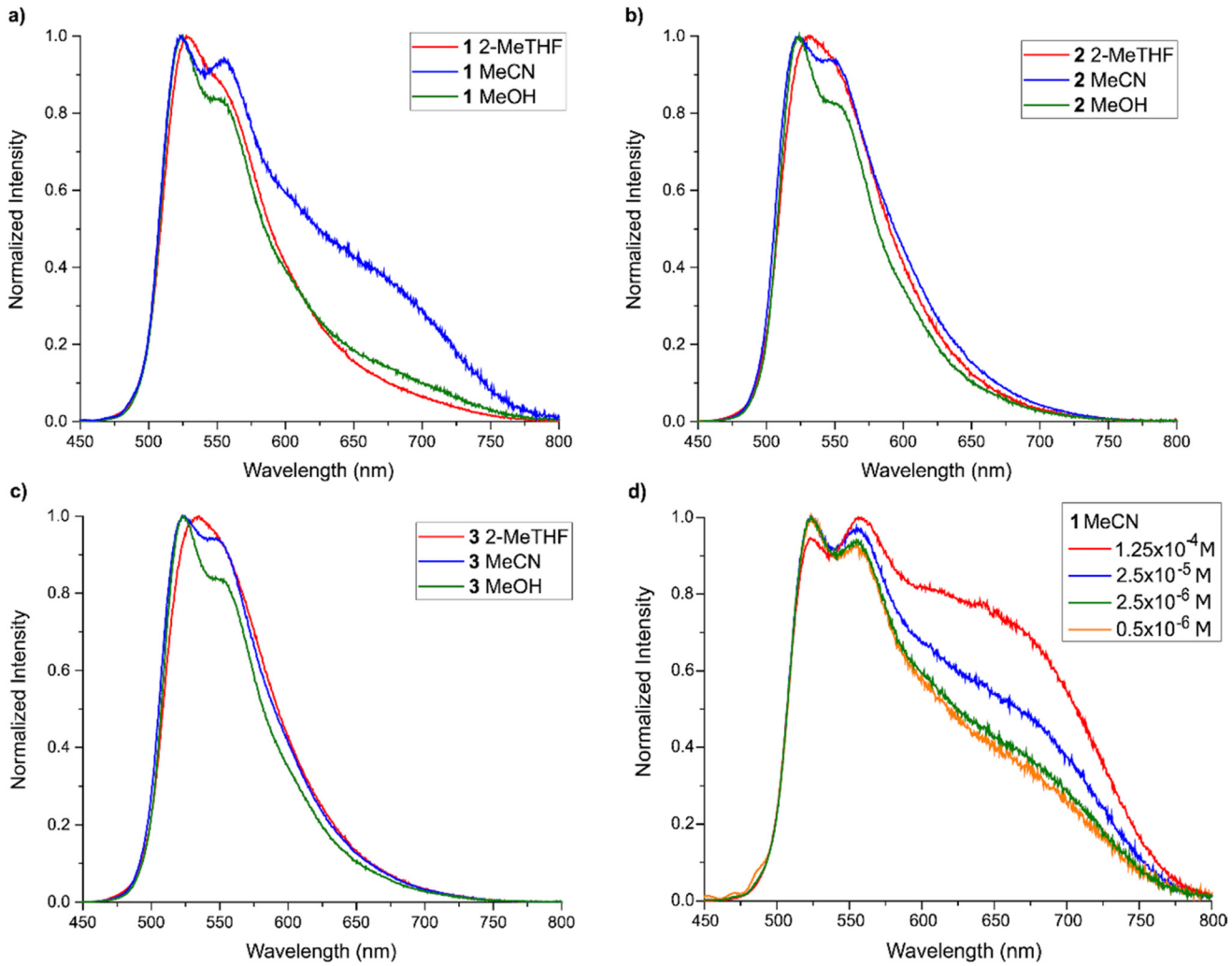

Fig. 6 Emission spectra of complexes **1** (a), **2** (b) and **3** (c) in different solvents at *ca.* 2.5 × 10^{-5} M concentration. (d) Emission spectra of complex **1** in MeCN solution at different concentrations (1.25 × 10^{-4} to 0.5 × 10^{-6} M).

Table 3 Emission data for the studied complexes

Complex	Medium	λ_{em} [a] (nm)	Φ [b]	τ [c] (μs)	$k_r \times 10^{-4}$ [d] (s^{-1})	$k_{nr} \times 10^{-4}$ [e] (s^{-1})
1	MeCN	*524*, 555, 670	0.12	1.3 (13%) 10.0 (87%)	1.4	9.9
	2-MeTHF	*529*, 556	0.39	4.3 (13%) 11.6 (87%)	3.6	5.8
	MeOH	*525*, 557, 678	0.05	1.7 (20%) 8.0 (80%)	0.7	14
	PMMA	*525*, 551	0.77	13.9	5.5	1.7
2	MeCN	*524*, 548	0.32	7.8	4.1	8.7
	2-MeTHF	532	0.47	11.3	4.3	4.7
	MeOH	*524*, 552	0.26	5.2	4.9	14
	PMMA	*525*, 551	0.73	14.0	5.2	1.9
3	MeCN	*524*, 548	0.59	9.3	6.3	4.4
	2-MeTHF	535	0.63	13.0	4.8	2.9
	MeOH	*523*, 551	0.49	7.2	6.8	7.1
	PMMA	*525*, 551	0.75	13.4	5.6	1.9
[Pt(dmtppy)(imz)]	2-MeTHF	533	0.73	14.3	5.1	1.9
	PMMA[f]	*521*, 548	0.71	14.0	5.1	2.1

[a] The most intense peak is italicized. [b] Phosphorescence quantum yield. [c] Lifetime. [d] Radiative rate constant, $k_r = \Phi/\tau$. [e] Nonradiative rate constant, $k_{nr} = (1 - \Phi)/\tau$. [f] Data from ref. 47.

Conclusions

Three Pt(II) dimers bearing an N^C^C heteroaromatic ligand and di-imidazolylidene ligands containing aliphatic linkers of different lengths have been synthesized. In all cases, they are obtained as a mixture of two atropisomers, which could only be separated when the linker between the NHC moieties is a methylene group. Based on their absorption and emission properties and DFT modelling, the {Pt(dmtppy)} units do not establish persistent intramolecular noncovalent interactions.

Highly intense phosphorescent emissions can be achieved in solution and PMMA matrices at 298 K, which are assigned to ^{3}ILCT/MLCT excited states of the individual, non-interacting {Pt(dmtppy)} units. The efficiencies in solution are strongly affected by the solvent. Thus, in the case of the shortest linker (complex **1**), the use of MeCN or MeOH favors the formation of excimers that cause a significant quenching of the emissions, whereas this is not observed in 2-MeTHF. Additionally, higher emission efficiencies in 2-MeTHF are achieved as the length of the linker increases, possibly because an intramolecular quenching mechanism is favored for the shorter linkers.

Experimental section

General considerations and materials

The dinuclear silver precursors $[Ag_2Br_2\{\mu\text{-}(Im_{Me})_2(CH_2)_n\}]$ (n = 1, 3, 6)[52] and complex $Bu_4N[PtCl(dmtppy)]$[46] were synthesized according to the reported methods. Synthesis-grade solvents were obtained from commercial sources. Elemental analyses were determined using a LECO CHNS-932 microanalyzer. NMR spectra were registered on a 600 MHz Bruker Avance spectrometer at room temperature. Chemical shifts are referred to residual signals of non-deuterated solvents and are given in ppm downfield from tetramethylsilane.

General procedure for the synthesis of complexes $[\{Pt(dmtppy)\}\{\mu\text{-}(Im_{Me})_2(CH_2)_n\}]$ (n = 1, 3, 6) (1–3)

A Carius tube was charged with $Bu_4N[PtCl(dmtppy)]$ (100 mg, 0.124 mmol), $[Ag_2Br_2\{\mu\text{-}(Im_{Me})_2(CH_2)_n\}]$ (n = 1, 3, 6) (0.069 mmol) and 1,2-dichloroethane (10 mL) and the mixture was heated at 80 °C for 90 min in the dark under an N_2 atmosphere. The solvent was removed under reduced pressure and the residue was filtered through silica gel using CH_2Cl_2 as solvent. The yellow fraction was collected and concentrated (2 mL), and hexane (10 mL) was added. The yellow precipitate was collected by filtration, washed with hexane (2 × 3 mL) and vacuum-dried to give **1–3**.

Data for complex 1. Yellow solid, obtained from $Bu_4N[PtCl(dmtppy)]$ (100 mg, 0.124 mmol) and $[Ag_2Br_2\{\mu\text{-}(Im_{Me})_2(CH_2)\}]$ (38 mg, 0.069 mmol). Yield: 42 mg (55%). HRMS (electrospray, m/z) calcd for $C_{59}H_{51}N_6Pt_2$ $[M + H]^+$: 1233.3451. Found: 1233.3455. Anal. calcd for $C_{59}H_{50}N_6Pt_2$: C, 57.46; H, 4.09; N, 6.81. Found: C, 57.56; H, 4.38; N, 6.52.

The separation of atropisomers was performed by column chromatography on silica gel using a $Et_2O/CHCl_3$ mixture (9 : 1) as the eluent. R_f atropisomer **1a** = 0.80; R_f atropisomer **1b** = 0.65.

Atropisomer **1a**. ^{1}H NMR (600 MHz, CD_2Cl_2): δ 8.13 (d, J_{H-H} = 5.2 Hz, 2H, CH), 7.93 (br td, J_{H-H} ~ 8.2, 1.5 Hz, 2H, CH), 7.90 (br d, J_{H-H} ~ 7.8 Hz, 2H, CH), 7.79 (d, J_{H-H} = 2.1 Hz, 2H, CH), 7.63–7.60 (m, 4H, CH), 7.60 (d, J_{H-H} = 1.3 Hz, 2H, CH), 7.53 (d, J_{H-H} = 1.4 Hz, 2H, CH), 7.32 (d, J_{H-H} = 7.5 Hz, 2H, CH), 7.29 (br d, J_{H-H} ~ 7.7 Hz, 4H, CH), 7.08 (br t, J_{H-H} ~ 6.4 Hz, 2H, CH), 6.90 (d, J_{H-H} = 13.3 Hz, 1H, CH_2), 6.86 (d, J_{H-H} = 13.3 Hz, 1H, CH_2), 6.82 (d, J_{H-H} = 2.1 Hz, 2H, CH) 6.79 (br d, J_{H-H} ~ 7.6 Hz, 2H, CH), 6.49 (br s with satellites, J_{Pt-H} = 73 Hz, 2H, CH), 3.84 (s, 6H, CH_3), 2.41 (s, 6H, CH_3), 2.10 (s, 6H, CH_3). $^{13}C\{^1H\}$ APT NMR (151 MHz, CD_2Cl_2): δ 195.3 (C), 179.2 (C), 169.1 (C), 156.0 (C), 154.6 (C), 152.3 (CH), 145.5 (C), 143.7 (C), 140.7 (C), 139.9 (CH), 138.4 (CH), 137.2 (C), 136.5 (C), 136.2 (C), 129.7 (CH), 127.1 (CH), 125.8 (CH), 124.6 (CH), 123.5 (CH), 122.2 (CH), 120.4 (CH), 119.8 (CH), 119.2 (CH), 118.9 (CH), 62.5 (CH_2), 37.9 (CH_3), 21.7 (CH_3), 21.2 (CH_3). $^{195}Pt\{^1H\}$ NMR (129 MHz, CD_2Cl_2): δ −3838.3 (s).

Atropisomer **1b**. ^{1}H NMR (600 MHz, CD_2Cl_2): δ 8.03 (ddd, J_{H-H} = 5.4, 1.6, 0.9 Hz, 2H, CH), 7.90–7.84 (m, 4H, CH), 7.76 (br s, 2H, CH), 7.64–7.60 (m, 4H, CH), 7.58 (br d, J_{H-H} ~ 1.2 Hz, 2H, CH), 7.54 (d, J_{H-H} = 1.3 Hz, 2H, CH), 7.34 (d, J_{H-H} = 7.6 Hz, 2H, CH), 7.29 (br d, J_{H-H} ~ 7.7 Hz, 4H, CH), 7.00 (br t, J_{H-H} ~ 6.4 Hz, 2H, CH), 6.93 (br s, 2H, CH_2), 6.86 (br s, 2H, CH), 6.83 (br d, J_{H-H} ~ 7.6 Hz, 2H, CH), 6.62 (br s with satellites, J_{Pt-H} = 69 Hz, 2H, CH), 3.84 (s, 6H, CH_3), 2.41 (s, 6H, CH_3), 2.18 (s, 6H, CH_3). $^{13}C\{^1H\}$ APT NMR (151 MHz, CD_2Cl_2): δ 195.3 (C), 179.2 (C), 169.0 (C), 156.1 (C), 154.6 (C), 152.3 (CH), 145.5 (C), 143.7 (C), 140.7 (C), 140.0 (CH), 138.2 (CH), 137.2 (C), 136.5 (C), 136.4 (C), 129.7 (CH), 127.0 (CH), 125.8 (CH), 124.7 (CH), 123.4 (CH), 120.9 (CH), 120.5 (CH), 119.7 (CH), 119.2 (CH), 118.9 (CH), 62.4 (CH_2), 37.9 (CH_3), 21.7 (CH_3), 21.2 (CH_3). $^{195}Pt\{^1H\}$ NMR (129 MHz, CD_2Cl_2): δ −3838.3 (s).

Data for complex 2. Yellow solid obtained from $Bu_4N[PtCl(dmtppy)]$ (100 mg, 0.124 mmol) and $[Ag_2Br_2\{\mu\text{-}(Im_{Me})_2(CH_2)_3\}]$ (40 mg, 0.069 mmol). Yield: 49 mg (63%). HRMS (electrospray, m/z) calcd for $C_{61}H_{55}N_6Pt_2$ $[M + H]^+$: 1261.3764. Found: 1261.3740. Anal. calcd for $C_{61}H_{54}N_6Pt_2$: C, 58.09; H, 4.32; N, 6.66. Found: C, 58.20; H, 4.52; N, 6.62. ^{1}H NMR (600 MHz, CD_2Cl_2): δ 8.12 (ddd, J_{H-H} = 5.4, 1.5, 0.8 Hz, 1H, CH), 8.06 (ddd, J_{H-H} = 5.4, 1.4, 0.8 Hz, 1H, CH), 7.90–7.79 (m, 4H, CH), 7.63–7.60 (m, 4H, CH), 7.57 (d, J_{H-H} = 1.2 Hz, 1H, CH), 7.54 (d, J_{H-H} = 1.3 Hz, 1H, CH), 7.53–7.51 (m, 2H, CH), 7.33–7.26 (m, 6H, CH), 6.97 (ddd, J_{H-H} = 7.1, 5.4, 1.7 Hz, 1H, CH), 6.95 (d, J_{H-H} = 2.0 Hz, 1H, CH), 6.93 (ddd, J_{H-H} = 7.1, 5.5, 2.0 Hz, 1H, CH), 6.86–6.84 (m, 2H, CH), 6.81–6.76 (m, 3H, CH), 6.49 (s with satellites, J_{Pt-H} = 73 Hz, 1H, CH), 6.42 (s with satellites, J_{Pt-H} = 73 Hz, 1H, CH), 4.30–4.16 (m, 4H, CH_2), 3.78 (s, 3H, CH_3), 3.76 (s, 3H, CH_3), 2.60–2.45 (m, 2H, CH_2), 2.40 (s, 6H, CH_3) 2.16 (s, 3H, CH_3), 2.10 (s, 3H, CH_3). $^{13}C\{^1H\}$ APT NMR (151 MHz, CD_2Cl_2): δ 193.8 (J_{Pt-C} = 874 Hz, C), 180.1 (J_{Pt-C} ~ 760 Hz, C), 180.0 (J_{Pt-C} ~ 760 Hz, C), 169.1 (J_{Pt-C} = 80 Hz, C), 156.0 (J_{Pt-C} = 120 Hz, C), 154.6 (C), 154.5 (C), 152.4 (CH), 152.3 (CH), 146.0 (J_{Pt-C} = 1180 Hz, C), 145.9 (J_{Pt-C} = 1180 Hz, C), 143.6 (C), 143.5 (C), 140.9 (C), 139.7 (J_{Pt-C} ~ 60 Hz, CH), 139.6

(J_{Pt-C} ~ 60 Hz, CH), 138.0 (CH), 137.9 (CH), 136.8 (C), 136.4 (C), 136.0 (C), 135.9 (C), 129.7 (CH), 127.0 (CH), 124.3 (CH), 124.2 (CH), 123.3 (CH), 123.2 (CH), 121.6 (CH), 121.0 (CH), 120.7 (CH), 120.3 (J_{Pt-C} = 66 Hz, CH), 119.6 (CH), 118.9 (CH), 118.7 (CH), 47.9 (CH_2), 47.8 (CH_2), 37.8 (CH_3), 37.7 (CH_3), 32.0 (CH_2), 31.9 (CH_2), 21.8 (CH_3), 21.7 (CH_3), 21.2 (CH_3). $^{195}Pt\{^1H\}$ NMR (129 MHz, CD_2Cl_2): δ −3823.2 (s), −3825.8 (s).

Data for complex 3. Yellow solid obtained from Bu_4N[PtCl(dmtppy)] (100 mg, 0.124 mmol) and [Ag_2Br_2{μ-(Im_{Me})$_2$(CH_2)$_6$}] (43 mg, 0.069 mmol). Yield: 51 mg (63%). HRMS (electrospray, *m*/*z*) calcd for $C_{64}H_{61}N_6Pt_2$ $[M + H]^+$: 1303.4234. Found: 1303.4165. Anal. calcd for $C_{64}H_{60}N_6Pt_2$: C, 58.98; H, 4.64; N, 6.45. Found: C, 58.89; H, 4.53; N, 6.49. ^1H NMR (600 MHz, CD_2Cl_2): δ 8.11 (dt, J_{H-H} = 5.1, 1.6 Hz, 1H, CH), 8.07 (dt, J_{H-H} = 5.5, 1.2 Hz, 1H, CH), 7.87–7.81 (m, 2H, CH), 7.80–7.76 (m, 2H, CH), 7.62–7.58 (m, 4H, CH), 7.55 (d, J_{H-H} = 1.2 Hz, 1H, CH), 7.52 (d, J_{H-H} = 1.2 Hz, 1H, CH), 7.50–7.48 (m, 2H, CH), 7.31–7.25 (m, 6H, CH), 7.01–6.98 (m, 2H, CH), 6.96–6.93 (m, 2H, CH), 6.90 (d, J_{H-H} = 1.9, 1H, CH), 6.85 (d, J_{H-H} = 1.9 Hz, 1H, CH), 6.78–6.74 (m, 2H, CH), 6.48 (d with satellites, J_{H-H} = 1.2 Hz, J_{Pt-H} = 73.0 Hz, 1H, CH), 6.45 (d with satellites, J_{H-H} = 1.2 Hz, J_{Pt-H} = 73.0 Hz, 1H, CH), 4.17–4.08 (m, 2H, CH_2), 4.06–3.95 (m, 2H, CH_2), 3.81 (s, 3H, CH_3), 3.79 (s, 3H, CH_3), 2.40 (s, 6H, CH_3), 2.14 (s, 3H, CH_3), 2.11 (s, 3H, CH_3), 1.64–1.56 (m, 4H, CH_2), 1.16–1.06 (m, 4H, CH_2). $^{13}C\{^1H\}$ APT NMR (151 MHz, CD_2Cl_2): δ 193.9 (J_{Pt-C} = 875 Hz, C), 180.3 (J_{Pt-C} = 753 Hz, C), 169.0 (C), 169.1 (C), 155.9 (J_{Pt-C} = 118 Hz, C), 154.7 (J_{Pt-C} = 142 Hz, C), 152.3 (CH), 146.1 (J_{Pt-C} = 1180 Hz, C), 146.0 (J_{Pt-C} = 1180 Hz, C), 143.5 (J_{Pt-C} = 42 Hz, C), 140.9 (C), 139.8 (CH), 139.7 (CH), 138.0 (CH), 136.7 (C), 136.6 (C), 136.4 (C), 135.8 (J_{Pt-C} = 70 Hz, C), 129.7 (CH), 127.0 (CH), 124.1 (CH), 123.1 (CH), 121.6 (CH), 120.6 (CH), 120.5 (CH), 120.1 (J_{Pt-C} = 68 Hz, CH), 119.5 (CH), 118.9 (CH), 118.7 (CH), 50.2 (CH_2), 37.7 (CH_3), 30.5 (CH_2), 26.0 (CH_2), 25.9 (CH_2), 21.8 (CH_3), 21.2 (CH_3). $^{195}Pt\{^1H\}$ NMR (129 MHz, CD_2Cl_2): δ −3822.0 (s).

Author contributions

M. P.: investigation, formal analysis. D. P.: investigation, formal analysis and supervision. P. G.-H.: software, supervision, formal analysis, funding acquisition, writing – review & editing. A. V.: conceptualization, investigation, methodology, data curation, supervision, validation, funding acquisition, writing – original draft, writing – review & editing.

Conflicts of interest

There are no conflicts to declare.

Data availability

Supplementary information (SI): variable temperature NMR experiments, NMR spectra of ^1H, $^{13}C\{^1H\}$ APT and ^{195}Pt, UV-Vis graphics for the photostability experiments, emission and excitation spectra and computational details and data. See DOI: https://doi.org/10.1039/d5dt01761k.

Acknowledgements

Financial support was provided by grant IJC2019-039057-I funded by MCIN/AEI/10.13039/501100011033 and "ESF Investing in your future", and grant 22074/JLI/22, funded by Fundación Séneca-Agencia de Ciencia y Tecnología de la Región de Murcia (Ayudas a Proyectos para la Generación de Nuevo Liderazgo Científico "Jóvenes Líderes en Investigación"). Grant PID2021-122966NB-I00 funded by MCIN/AEI/10.13039/501100011033 and "ERDF A way of making Europe" is also acknowledged.

References

1 J. Herberger and R. F. Winter, *Coord. Chem. Rev.*, 2019, **400**, 213048.
2 K. Li, G. S. M. Tong, Q. Wan, G. Cheng, W. Y. Tong, W. H. Ang, W. L. Kwong and C. M. Che, *Chem. Sci.*, 2016, **7**, 1653–1673.
3 Y. Chi and P. T. Chou, *Chem. Soc. Rev.*, 2010, **39**, 638–655.
4 S. Y. Yang, Y. Chen, R. T. K. Kwok, J. W. Y. Lam and B. Z. Tang, *Chem. Soc. Rev.*, 2024, **53**, 5366–5393.
5 Y. C. Wei, K. H. Kuo, Y. Chi and P. T. Chou, *Acc. Chem. Res.*, 2023, **56**, 689–699.
6 L. Le Bras, K. Chaitou, S. Aloïse, C. Adamo and A. Perrier, *Phys. Chem. Chem. Phys.*, 2019, **21**, 46–56.
7 C. Li and J. Zhao, *Inorg. Chem.*, 2024, **63**, 11757–11767.
8 A. Lázaro, R. Bosque, J. S. Ward, K. Rissanen, M. Crespo and L. Rodríguez, *Inorg. Chem.*, 2023, **62**, 2000–2012.
9 M. Martínez-Junquera, E. Lalinde and M. T. Moreno, *Inorg. Chem.*, 2022, **61**, 10898–10914.
10 O. S. Wenger, *Chem. Rev.*, 2013, **113**, 3686–3733.
11 A. Kobayashi and M. Kato, *Eur. J. Inorg. Chem.*, 2014, **2014**, 4469–4483.
12 Y. S. Wong, M. Ng, M. C. L. Yeung and V. W. W. Yam, *J. Am. Chem. Soc.*, 2021, **143**, 973–982.
13 M. Yoshida and M. Kato, *Anal. Sci.*, 2025, **41**, 1233–1249.
14 E. V. Puttock, M. T. Walden and J. A. G. Williams, *Coord. Chem. Rev.*, 2018, **367**, 127–162.
15 H. B. Gray, S. Záliš and A. Vlček, *Coord. Chem. Rev.*, 2017, **345**, 297–317.
16 I. Melendo, S. Fuertes, A. Martín and V. Sicilia, *Inorg. Chem.*, 2024, **63**, 5470–5480.
17 S. Chakraborty, A. Aliprandi and L. De Cola, *Chem. – Eur. J.*, 2020, **26**, 11007–11012.
18 H. Zhang, C. Liu, J. Zhang, C. X. Du and B. Zhang, *Organometallics*, 2022, **41**, 1381–1390.
19 L. Wang, Z. Wen, Y. Xu, Y. Zhang, J. Miao, Z. Chen and K. Li, *Mater. Chem. Front.*, 2023, **7**, 873–880.

20 P. Pinter, J. Soellner and T. Strassner, *Eur. J. Inorg. Chem.*, 2021, **2021**, 3104–3107.
21 V. Sicilia, L. Arnal, D. Escudero, S. Fuertes and A. Martin, *Inorg. Chem.*, 2021, **60**, 12274–12284.
22 K. W. Lo, G. S. M. Tong, G. Cheng, K. H. Low and C. M. Che, *Angew. Chem., Int. Ed.*, 2022, **61**, e202115515.
23 A. W. Mills, A. J. S. Valentine, K. Hoang, S. Roy, F. N. Castellano, L. X. Chen and X. Li, *J. Phys. Chem. A*, 2021, **125**, 9438–9449.
24 T. Han, J. Ren, S. Jiang, F. Wang and Y. Tian, *Inorg. Chem.*, 2024, **63**, 11523–11530.
25 S. Y. L. Leung, A. Y. Y. Tam, C. H. Tao, H. S. Chow and V. W. W. Yam, *J. Am. Chem. Soc.*, 2012, **134**, 1047–1056.
26 G. Romo-Islas, R. M. Gomila, A. Frontera and L. Rodríguez, *Inorg. Chem. Front.*, 2023, **10**, 6204–6220.
27 W. Lu, M. C. W. Chan, N. Zhu, C. M. Che, C. Li and Z. Hui, *J. Am. Chem. Soc.*, 2004, **126**, 7639–7651.
28 R. W. Y. Sun, A. L. F. Chow, X. H. Li, J. J. Yan, S. S. Y. Chui and C. M. Che, *Chem. Sci.*, 2011, **2**, 728–736.
29 G. Wang, K. Feng, M. J. Crossley, L. Xing, H. Xiao, W. Li, C.-H. Tung and L.-Z. Wu, *Chem. – Eur. J.*, 2016, **22**, 11962–11966.
30 X. P. Zhang, L. L. Wang, X. W. Qi, D. S. Zhang, Q. Y. Yang, Z. F. Shi, Q. Lin and T. Wu, *Dalton Trans.*, 2018, **47**, 10179–10186.
31 M. A. Esteruelas, S. Moreno-Blázquez, M. Oliván and E. Oñate, *Inorg. Chem.*, 2024, **63**, 14482–14494.
32 P. Pander, M. T. Walden, R. J. Salthouse, A. Sil, D. S. Yufit, F. B. Dias and J. A. G. Williams, *J. Mat. Chem. C*, 2023, **11**, 15335–15346.
33 F. K. W. Kong, A. K. W. Chan, M. Ng, K. H. Low and V. W. W. Yam, *Angew. Chem., Int. Ed.*, 2017, **56**, 15103–15107.
34 S. Bellemin-Laponnaz, *Eur. J. Inorg. Chem.*, 2020, **2020**, 10–20.
35 S. Zhao, Z. Yang, G. Jiang, S. Huang, M. Bian, Y. Lu and W. Liu, *Coord. Chem. Rev.*, 2021, **449**, 214217.
36 T. Jia, O. Diane, D. Ghosh, M. Skander, G. Fontaine, P. Retailleau, J. Poupon, J. Bignon, Y. M. Moulai Siasia, V. Servajean, N. Hue, J. F. Betzer, A. Marinetti and S. Bombard, *J. Med. Chem.*, 2023, **66**, 6836–6848.
37 M. Bouché, A. Bonnefont, T. Achard and S. Bellemin-Laponnaz, *Dalton Trans.*, 2018, **47**, 11491–11502.
38 R. Visbal and M. C. Gimeno, *Chem. Soc. Rev.*, 2014, **43**, 3551–3574.
39 H. Amouri, *Chem. Rev.*, 2023, **123**, 230–270.
40 J. Soellner and T. Strassner, *Chem. – Eur. J.*, 2018, **24**, 15603–15612.
41 R. Kumar, A. Linden and C. Nevado, *Angew. Chem., Int. Ed.*, 2015, **54**, 14287–14290.
42 W. Feuerstein, C. Holzer, X. Gui, L. Neumeier, W. Klopper and F. Breher, *Chem. – Eur. J.*, 2020, **26**, 17156–17164.
43 C. Y. Wong, S. L. Lai, M. Y. Leung, M. C. Tang, L. K. Li, M. Y. Chan and V. W. W. Yam, *J. Am. Chem. Soc.*, 2023, **145**, 2638–2646.
44 W. Feuerstein and F. Breher, *Chem. Commun.*, 2020, **56**, 12589–12592.
45 V. Höhn, W. Feuerstein, F. R. Rehak, M. Kehry, S. Lebedkin, M. M. Kappes, W. Klopper and F. Breher, *Inorg. Chem.*, 2023, **62**, 15627–15640.
46 D. Poveda, Á. Vivancos, D. Bautista and P. González-Herrero, *Inorg. Chem.*, 2023, **62**, 6207–6213.
47 D. Poveda, Á. Vivancos, D. Bautista and P. González-Herrero, *Inorg. Chem.*, 2023, **62**, 20987–21002.
48 C. P. Newman, R. J. Deeth, G. J. Clarkson and J. P. Rourke, *Organometallics*, 2007, **26**, 6225–6233.
49 S. Burling, S. Douglas, M. F. Mahon, D. Nama, P. S. Pregosin and M. K. Whittlesey, *Organometallics*, 2006, **25**, 2642–2648.
50 V. H. Nguyen, T. T. Dang, H. H. Nguyen and H. V. Huynh, *Organometallics*, 2020, **39**, 2309–2319.
51 Á. Vivancos, D. Bautista and P. González-Herrero, *Inorg. Chem.*, 2022, **61**, 12033–12042.
52 J. Gil-Rubio, V. Cámara, D. Bautista and J. Vicente, *Organometallics*, 2012, **31**, 5414–5426.